

# Implications of DES 5YR SNe Dataset for $\Lambda$ CDM

Eoin Ó Colgáin,<sup>1</sup> Saeed Pourojaghi,<sup>2</sup> and M. M. Sheikh-Jabbari<sup>3</sup>

<sup>1</sup>*Atlantic Technological University, Ash Lane, Sligo F91 YW50, Ireland*

<sup>2</sup>*Department of Physics, Bu-Ali Sina University, Hamedan 65178, Iran*

<sup>3</sup>*School of Physics, Institute for Research in Fundamental Sciences (IPM), P.O.Box 19395-5531, Tehran, Iran*

Dark Energy Survey five-year supernovae data (DES 5YR SNe) in conjunction with Planck CMB and Dark Energy Spectroscopic Instrument (DESI) BAO data has detected a strong dynamical dark energy deviation from the  $\Lambda$ CDM model. Here we shift the focus of DES data to the pressureless matter sector in the  $\Lambda$ CDM model by studying the matter density parameter  $\Omega_m$ . Employing frequentist profile likelihoods, we demonstrate that  $\Omega_m$  increases with effective redshift in the DES data at up to  $2.5\sigma$  discrepant with Planck. At the highest redshifts, one encounters negative dark energy densities  $\Omega_m > 1$ . Our findings corroborate earlier observations in Pantheon and Pantheon+ datasets with an independent SNe dataset with a higher effective redshift. In an appendix, we confirm that curvature  $\Omega_k$  decreases with effective redshift disfavours a flat Universe in higher redshift DES SNe at  $> 3\sigma$ . Our choice of  $\Omega_k$  prior leads to an underestimation of the tension with a flat Universe.

## I. INTRODUCTION

In recent years, cosmological or  $\Lambda$ CDM tensions have caused considerable confusion (see [1–3] for reviews). Given a physical discrepancy - one not due to systematics - in the Hubble constant  $H_0$  assuming the  $\Lambda$ CDM model, the simplest deduction one can make is that the  $\Lambda$ CDM fitting parameter  $H_0$ <sup>1</sup> must not be a constant, i. e. it depends on the redshift at which it is measured [4, 5]. This begets a research programme where one studies  $H_0$  tomographically by confronting the  $\Lambda$ CDM model to data binned by effective redshift. To that end, descending trends of  $H_0$  with redshift in the late Universe have been synergistically reported in the literature for various different datasets [6–15].

$H_0$  does not exist in a vacuum; cosmologically, it must talk to other  $\Lambda$ CDM parameters. The next most relevant parameter is matter density today  $\Omega_m$ . This parameter is arguably no less special than  $H_0$ . In the baseline flat  $\Lambda$ CDM model,  $\Omega_m$  parameterises both the pressureless matter and dark energy sectors. Moreover, it is also the backbone of the  $\Lambda$ CDM model, describing the evolution of the Universe at the level of equations of motion over 13 billion years through a single parameter. Any textbook on cosmology confirms that the Universe is approximately 30% matter density corresponding to  $\Omega_m \approx 0.3$ . If this picture is correct,  $\Omega_m$  cannot drift far from  $\Omega_m \approx 0.3$ . Lastly,  $\Omega_m$  is anti-correlated with  $H_0$  when one fits data, so the flip side of the decreasing  $H_0$  with redshift narrative is an increasing  $\Omega_m$  with redshift narrative. Unsurprisingly, claims of increasing values of  $\Omega_m$  with effective redshift also exist in the literature [12, 13, 16–19]. See [20] for an overview of the claims.

An increasing  $\Omega_m$  with redshift, if physical, leads one to an “ $\Omega_m$  tension”. The most striking realisation comes from Risaliti-Lusso quasar (QSO) datasets [16, 17, 21], which has

recently been placed at  $\sim 8\sigma$  level with frequentist methods [22] (see also [23–25]). Coupled with  $H_0$  tension, a putative  $\sim 5\sigma$  tension [26], one could be looking at an existential crisis for the vanilla  $\Lambda$ CDM model. Understandably, given the strong disagreement with the standard model, the QSO dataset has been heavily criticised [24, 25, 27–31]. Nevertheless, the observation that  $\Omega_m$  increases with effective redshift in the flat  $\Lambda$ CDM model extends to Type Ia SNe [12, 13, 32], in particular Pantheon [33] and Pantheon+ [34, 35] samples. The problem with these samples is that at higher redshifts the samples become sparse and the  $z > 1$  SNe are common to Pantheon and Pantheon+<sup>2</sup>, preventing one from expanding the science case.

The Dark Energy Survey’s five year (DES 5YR) SNe sample [39] offers considerable promise. First, in contrast to QSOs, Type Ia SNe are better quality *standardisable* candles with greater community trust. Secondly, the DES sample has better high redshift statistics compared to Pantheon+ [34, 35] or Union3 [40]. Thirdly, deviations from  $\Lambda$ CDM behaviour have already been reported by the DES collaboration in the dark energy sector [39], a problem that is exacerbated by combining the dataset with DESI BAO [41] and Planck CMB constraints [42]. It is worth noting that between Pantheon+, Union3 and DES, the CMB+BAO+SNe signal for dynamical dark energy is  $2.5\sigma$ ,  $3.5\sigma$  and  $3.9\sigma$  level, respectively [41]. In DES data, this signal is driven by differences in the  $\Lambda$ CDM  $\Omega_m$  parameter with the dark energy sector compensating, as is evident from Fig. 8 of ref. [39]<sup>3</sup>.

In this letter, we confirm existing results in the literature that  $\Omega_m$  increases with effective redshift in the *independent* DES 5YR sample. Noting that the parameter  $\Omega_m$  is common to both the dark energy and pressureless matter sectors, neglecting a DES SNe systematic, this implies that the  $\Lambda$ CDM cosmology is incorrectly modelling one if not both of the sec-

<sup>1</sup> $H_0$  is the only cosmological parameter that can be determined model independently just upon the assumption of cosmic homogeneity and isotropy, by extrapolating low redshift data  $z \lesssim 0.1$  to  $z = 0$ . At higher redshifts, one may assume a Taylor expansion in  $z$  and the first term is then acceleration parameter. Asking for Hubble parameter at arbitrary redshift  $H(z)$  requires a cosmological model.

<sup>2</sup>Pantheon+ cuts 57 high redshift SNe from the SNLS sample [36, 37] due to potential evolution in inferred distances [38], so Pantheon+ statistics are worse than Pantheon at higher redshifts.

<sup>3</sup>Puzzlingly,  $w(z=0) = w_0$  is consistent with zero within  $1\sigma$  [39], thus problematic for late-time accelerated expansion today. Moreover, the Universe is younger by 9% or 1.3 gigayears with dynamical dark energy [39].

tors. Ultimately, the surprise is not that  $\Omega_m$  varies between CMB, BAO and SNe datasets [41], but that it can vary within a single (SNe) dataset when it is analysed tomographically.

## II. METHODOLOGY

Here, we use frequentist confidence intervals based on profile likelihood ratios (see [43] for a review) to track differences in cosmological fitting parameters. We use two methodologies. The first is based on Wilks' theorem [44] and assumes that the profile likelihood is Gaussian, an assumption that is valid in the large sample limit; the DES SNe sample is large and one can safely apply Wilks' theorem. The second is based on a method that is applicable to non-Gaussian profile likelihoods [22, 45, 46], yet is guaranteed to recover results consistent with Wilks' theorem in the Gaussian regime.

On the data side, we analyse the DES 5YR sample [39] of 1829 SNe, 194 of which are common to CfA [47, 48], CSP [49] and Foundation samples [50], leaving 1635 independent SNe in the DES sample. What interests us here is that the sample has a higher effective redshift than Pantheon+ [34, 35]. In short, we repeat the analysis of [32] but with the independent DES sample with better statistics at higher redshifts.

We are interested in the flat  $\Lambda$ CDM model with Hubble parameter,

$$H(z) = H_0 \sqrt{1 - \Omega_m + \Omega_m(1+z)^3}, \quad (1)$$

where  $H_0$  is the Hubble constant and  $\Omega_m$  is the matter density parameter. We treat both as fitting parameters. From here, one constructs the luminosity distance  $D_L(z)$

$$D_L(z) = \frac{c}{H_0} (1+z) \chi(z), \quad \chi(z) := \int_0^z \frac{H_0}{H(z')} dz', \quad (2)$$

which appears in the distance modulus:

$$\mu(z) = 5 \log_{10} D_L(z) + 25. \quad (3)$$

To fit DES 5YR data, we consider the  $\chi^2$ -likelihood:

$$\chi^2 = \Delta\mu_i C_{ij}^{-1} \Delta\mu_j, \quad (4)$$

where  $C_{ij}$  is the  $1829 \times 1829$  covariance matrix incorporating statistical and systematic uncertainties [39] and  $\Delta\mu_i = \mu(z_i) - \mu_i$  is the difference between the model prediction at redshift  $z_i$  and the observed distance modulus  $\mu_i$ . The DES collaboration provide Hubble diagram redshifts, distance moduli and the corresponding distance moduli errors  $\sigma_{\mu_i}$  [39]. We added  $\sigma_{\mu_i}^2$  to the diagonal of the covariance matrix provided by DES. This is validated later by recovering DES results.

At this juncture, we depart from DES analysis by employing profile likelihoods in place of Markov Chain Monte Carlo (MCMC). As we shall see, for the full sample, either with or without 194 external SNe [47–50], we recover DES results. This provides an important consistency check on our methods. Profile likelihoods for one degree of freedom  $\theta$  are constructed by isolating one of the parameters  $\theta \in \{H_0, \Omega_m\}$  and scanning over it while maximising the likelihood  $\mathcal{L} \propto e^{-\frac{1}{2}\chi^2}$

with respect to the other parameter. Here, we focus on  $\Omega_m$  and maximise with respect to  $H_0$ . How  $H_0$  is calibrated is not an issue, it is simply a nuisance parameter in our analysis. The profile likelihood ratio for  $\Omega_m$  is [43]

$$R(\Omega_m) = \exp\left(-\frac{1}{2}(\chi_{\min}^2(\Omega_m) - \chi_{\min}^2)\right), \quad (5)$$

where  $\chi_{\min}^2(\Omega_m)$  is the minimum of the  $\chi^2$ , or alternatively maximum of the likelihood, for each value of  $\Omega_m$ , whereas  $\chi_{\min}^2$  is the global minimum of the  $\chi^2$  over all values of  $\Omega_m$  that we probe. The reader will note that the profile likelihood ratio (5) peaks at  $R(\Omega_m) = 1$  by construction.

With the profile likelihood ratio constructed, we employ two different methods to identify confidence intervals. The first *assumes* that the profile likelihood is Gaussian in the large sample limit [44]. One then identifies 100  $\alpha\%$  confidence intervals corresponding to the values of  $\Delta\chi^2$  satisfying [43]:

$$\alpha = \int_{y=0}^{y=\Delta\chi^2} \frac{1}{\sqrt{2\pi y}} e^{-\frac{1}{2}y} dy, \quad (6)$$

where we have specialised to the chi-squared distribution with one degree of freedom and employed  $\Gamma(\frac{1}{2}) = \sqrt{\pi}$ . Integrating the right hand side to  $\Delta\chi^2 = 1$  and  $\Delta\chi^2 = 3.9$  one finds  $\alpha = 0.6827$  and  $\alpha = 0.9517$ , corresponding to 68% and 95% confidence intervals, respectively.

Alternatively, one can construct, 68%, 95% confidence intervals for the profile likelihood, by normalising the profile likelihood ratio by the total area under the curve [45, 46],

$$w(\Omega_m) = \frac{R(\Omega_m)}{\int R(\Omega_m) d\Omega_m}, \quad (7)$$

and solving the equation

$$\int_{\Omega_m^{(1)}}^{\Omega_m^{(2)}} w(\Omega_m) d\Omega_m = \{0.68, 0.95\}, \quad w(\Omega_m^{(1)}) = w(\Omega_m^{(2)}). \quad (8)$$

It should be noted that (7) and (8) are essentially equations (2) and (3) from [51]. The content of (8) is that one builds confidence intervals outwards from the peak of the profile likelihood ratio or maximum likelihood estimator (MLE) by steadily including points in parameter space that are incrementally less likely until one reaches 68%, 95%, etc, of the area under the profile likelihood curve. It is apparent from the construction that when the profile likelihoods are close to Gaussian the two methods agree. We will show this explicitly for our case, but further explanations can be found in ref. [22].

We remark that there is a Feldman-Cousins prescription [52] for handling boundaries, i. e. priors imposed on parameters. Since the MLE or peak of our profile likelihood  $R(\Omega_m)$  is located at larger  $\Omega_m$  values than the Planck value  $\Omega_m \approx 0.3$ , and the boundary is at  $\Omega_m = 0$ , the boundary never impacts our lower confidence intervals or the inferred tensions. Thus, the Feldman-Cousin prescription is irrelevant. However, we do relax the usual  $\Omega_m \leq 1$  prior in order to identify the MLE for  $z > 0.8$  SNe. Imposing the  $\Omega_m \leq 1$  prior on  $z > 0.8$  SNe would reduce the tension with Planck, as happens with our

$\Omega_k$  priors in the appendix, but cannot impact redshift ranges where the MLE is in the range  $\Omega_m \in [0, 1]$ . Only by relaxing the priors can one judge if it is the prior or the data that is constraining the model.

### III. RESULTS

As a consistency check on our methodology, we first construct the profile likelihood for the full DES sample of 1829 SNe and recover  $\Omega_m = 0.352 \pm 0.17$  value from Table 2 [39]. Concretely, whether we employ the approximation  $\Delta\chi^2 \leq 1$  or integrate under the profile likelihood curve following (7) and (8), we find  $\Omega_m = 0.349^{+0.017}_{-0.016}$ . The profile likelihood ratio is illustrated in Fig. 1, where we have minimised the  $\chi^2$  in the range  $\Omega_m \in [0.3, 0.4]$  in steps of  $\Delta\Omega_m = 0.01$ . Note, we have discretised the  $\Omega_m$  parameter space and scanned over it, so our central value is accurate up to the  $\Delta\Omega_m = 0.01$  precision. Nevertheless, the important point here is that we agree with DES on the errors with independent methodology. This provides reassurance that we have properly propagated statistical and systematic uncertainties through the DES covariance matrix.

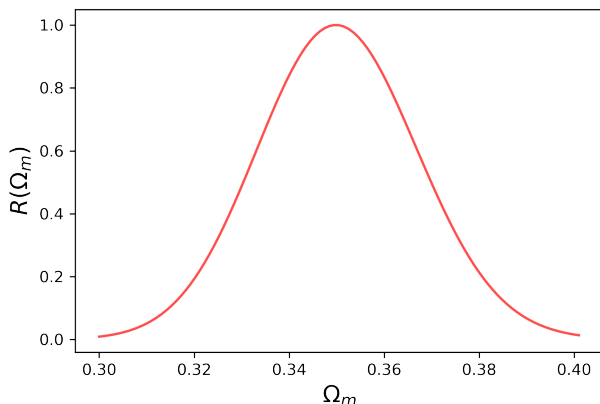


FIG. 1: The  $\Omega_m$  profile likelihood ratio for the full DES 5YR SNe sample of 1829 SNe.

Our next step follows [32] and involves truncating out the lowest redshift SNe and repeating the analysis. We focus on approximately 300  $\Omega_m$  values evenly spaced in the range  $\Omega_m \in [0, 3]$ . We start by removing the 194 SNe from datasets [47–50] external to DES and crop the covariance matrix accordingly. This leads to the first entry in Table I. Interestingly, the removal of external data shifts  $\Omega_m$  back closer to the Planck value [42]. Nevertheless, as is evident from Table I and Fig. 2, removing the lowest redshift SNe from exclusively DES data leads to larger values of  $\Omega_m$ . In particular, already for  $z > 0.5$  SNe we recover the higher  $\Omega_m \approx 0.35$  value preferred by the full sample. In addition, for  $z > 0.6$  SNe, a discrepancy is evident with canonical Planck values. From Table I and Fig. 2, it is evident that our two methods for constructing frequentist confidence intervals agree well provided the profile likelihoods are close to Gaussian and  $R(\Omega_m)$

falls off to small values within our priors. Nevertheless, of the two methods, confidence intervals based on (7) and (8) are more conservative. Evidently, the profile likelihoods become broader and more non-Gaussian at higher redshifts. We note that  $\Delta\chi^2 \leq 1$  corresponds to  $R(\Omega_m) \geq 0.607$ , so one can eyeball the confidence intervals by drawing a horizontal line in Fig. 2 at  $R(\Omega_m) \approx 0.6$ . It is clear that the red profile likelihood curve only intersects  $R(\Omega_m) \approx 0.6$  once within our bounds, so we only quote lower bounds in Table I. Anyone surprised by the result should look at Fig. 8 of [39], where it is evident that a dynamical dark energy sector is compensating larger  $\Omega_m$  values. Our findings here offer greater transparency.

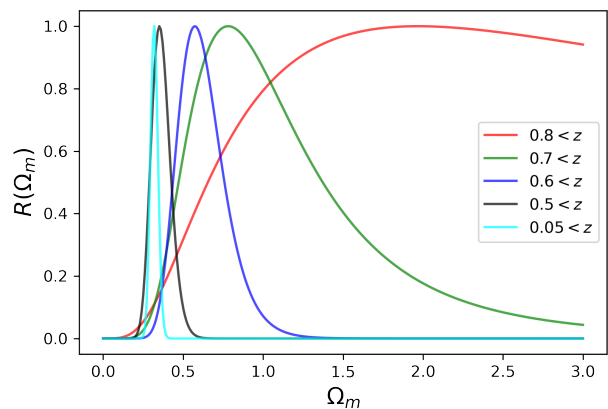


FIG. 2: Tomographic or redshift-binned profile likelihood ratios. The MLE shifts to larger values with increasing effective redshift. For the highest redshift range the MLE is in the negative dark energy density regime with  $\Omega_m > 1$ .

Redshift	# SNe	$\Omega_m$ (68%)	$\Omega_m$ ( $\Delta\chi^2 \leq 1$ )
0.05 < z	1635	$0.321^{+0.020}_{-0.020}$	$0.321^{+0.020}_{-0.020}$
0.5 < z	874	$0.351^{+0.070}_{-0.050}$	$0.351^{+0.060}_{-0.050}$
0.6 < z	554	$0.572^{+0.170}_{-0.120}$	$0.572^{+0.151}_{-0.110}$
0.7 < z	259	$0.783^{+0.592}_{-0.311}$	$0.783^{+0.472}_{-0.271}$
0.8 < z	128	$1.385 < (1.967)$	$0.763 < (1.967)$

TABLE I: 68% confidence intervals inferred with two methods from DES SNe in different redshift ranges. The number of SNe are also documented. For one-sided confidence intervals we record the MLE in brackets.

We can work out the disagreement with Planck for the  $1\sigma$  upper bound  $\Omega_m \leq 0.322$  [42]. We will do this by extracting  $\Delta\chi^2$  values and integrating the profile likelihood. Focusing on  $\Delta\chi^2$ , we identify the maximum value of  $R(\Omega_m)$  corresponding to the Planck  $1\sigma$  upper bound. The 1629 DES SNe sample in cyan in Fig. 2 is evidently within the Planck  $1\sigma$  confidence interval and only  $\Delta\chi^2 = 0.1$  removed from the Planck central value  $\Omega_m = 0.315$  [42], which makes it consistent at  $0.3\sigma$ . For DES SNe with redshifts  $z > 0.8$  (red curve), the Planck

$1\sigma$  upper bound corresponds to  $R(\Omega_m) \leq 0.111 \Leftrightarrow \Delta\chi^2 \geq 4.4$ , which disfavors the Planck value at 96.4% confidence level or  $\sim 2.1\sigma$ . For DES SNe with redshifts  $z > 0.7$  (green curve), the Planck values correspond to  $R(\Omega_m) \leq 0.109 \Leftrightarrow \Delta\chi^2 \geq 4.4$ , which again disfavors Planck at  $\sim 2.1\sigma$ . For DES SNe with redshifts  $z > 0.6$  (blue curve), we find  $R(\Omega_m) \leq 0.045 \Leftrightarrow \Delta\chi^2 \geq 6.2$ , which disfavors Planck at 98.7% confidence level or  $\sim 2.5\sigma$ . Finally, for DES SNe with redshifts  $z > 0.5$ , we have  $R(\Omega_m) \leq 0.858 \Leftrightarrow \Delta\chi^2 \geq 0.3$ , which is only  $\sim 0.5\sigma$  removed from Planck. It is worth noting that from the redshift ranges sampled, we find the largest discrepancy with Planck from a profile likelihood that is close to Gaussian, thus any deviation from Wilks' theorem is expected to be small.

We repeat the analysis by dropping the assumption of a Gaussian profile likelihood and integrate under the curve following (7) and (8). The full DES SNe sample (cyan curve) we find to be consistent with the Planck central value  $\Omega_m = 0.315$  at 16.7% confidence level or  $\sim 0.2\sigma$ . For DES SNe with  $z > 0.8$  (red curve), the Planck  $1\sigma$  upper bound appears at 99.6% confidence level or  $\sim 2.9\sigma$ . We note that this number differs considerably from  $\sim 2.1\sigma$  from Wilks' theorem, but this shows the impact of non-Gaussianities and the boundary. We anticipate that one can relax the  $\Omega_m \in [0, 3]$  bound and this would reveal a profile likelihood ratio that falls away gradually for larger  $\Omega_m$  values. What this will mean is that the area under the profile likelihood curve consistent with Planck  $\Omega_m$  values or smaller will be even less of the overall area, thus disfavoring Planck more. For DES SNe with  $z > 0.7$  (green curve), the Planck  $1\sigma$  upper bound is disfavoured at 95.4% confidence level or  $\sim 2\sigma$ . This compares favourably with  $\sim 2.1\sigma$  from Wilks' theorem. For DES SNe with  $z > 0.6$ , the Planck  $1\sigma$  upper bound is disfavoured at 98.4% confidence level or  $\sim 2.4\sigma$ , compared to  $\sim 2.5\sigma$  from our earlier analysis based on Wilks' theorem. We emphasise again that for close to Gaussian profile likelihoods the agreement is good. Finally, for  $z > 0.5$  DES SNe, we find the Planck  $1\sigma$  upper bound appears at 38.8% confidence level or  $\sim 0.5\sigma$ .

The main takeaway message from our analysis is that  $\Omega_m$  is not a constant in DES data, and as is evident from Fig. 2 and Table I, it increases with effective redshift. It should be evident from Fig. 8 in [39] that a larger  $\Omega_m$  value drives the dynamical dark energy signal.

#### IV. DISCUSSION

We remind the reader again that persistent  $\Lambda$ CDM tensions [1–3], in particular  $H_0$  tension [26], necessitate one finding changes in  $\Lambda$ CDM fitting parameters with effective redshift [4, 5]. This is an irrefutable signature of model breakdown. As reviewed recently in [22] with similar methodology, Risaliti-Lusso QSOs and gamma-ray burst (GRB) datasets exist that support  $\Omega_m$  increasing tomographically with redshift in the  $\Lambda$ CDM model. Nevertheless, at best, QSOs and GRBs are emerging cosmological probes [53], and their standardisability is too easy to question.

This is much more difficult to do with Type Ia SNe, the gold standard of cosmological distance indicators. Decreasing

$H_0$ /increasing  $\Omega_m$  trends have been observed in Type Ia SNe [8–15, 18, 19], in particular in Pantheon [33] and Pantheon+ [34, 35] samples. The problem therein is that at the highest redshifts the statistics are low. The new DES 5YR sample plugs this gap, yet in this letter we find a qualitatively similar increasing  $\Omega_m$  with effective redshift trend to QSOs/GRBs. We stress that our observations here should be unsurprising. Fig. 8 of [39] is evidently a funky plot; it should be obvious that a larger  $\Omega_m$  value is compensated by dynamical dark energy with potentially curious side effects, namely a lack of late-time accelerated expansion in Table 2 [39],  $w(z=0) = w_0 \sim 0$  within  $1\sigma$ , and a Universe younger by 9% [39]. We emphasise again that while we have adopted different methodology, we recovered DES results for the full sample. One could attribute the increasing  $\Omega_m$  trend with effective redshift to systematics in the DES sample or problems standardising Type Ia SNe at higher redshifts, however, given the difference in astrophysics with QSOs/GRBs, yet the same result [22], this demands that scrutiny falls on the  $\Lambda$ CDM model. Note,  $\Lambda$ CDM tensions [1–3] independently demand as much.

Given that we assume the  $\Lambda$ CDM model, yet find changes in  $\Omega_m$  with redshift, it is unclear if the problem concerns the pressureless matter or the dark energy sector. Nevertheless, we see greater deviations from the Planck  $\Omega_m$  value at higher redshifts, where dark energy is less relevant, so to first approximation this implies a problem in the matter dominated regime. While pressureless matter can be tested by ensuring that  $H(z)$  scales as  $H(z) \sim (1+z)^{\frac{3}{2}}$  at high redshifts in the matter-dominated regime, dynamical dark energy can be parameterised through a function  $f(z)$  in the Hubble parameter,  $H(z) = H_0 \sqrt{(1-\Omega_m)f(z) + \Omega_m(1+z)^3}$ , where  $f(0) = 1$  and at large  $z$ ,  $f(z) \sim z^a$ ,  $a < 2$ .  $f(z)$  in principle has infinite number of degrees of freedom and is hence an unfalsifiable paradigm. For this reason, we must first make sure that matter is pressureless before one buys a function  $f(z)$  in  $H(z)$ . See [54, 55] for a sample of functions  $f(z)$  confronted to DES SNe that are discrepant with  $\Lambda$ CDM behaviour. *A priori*, nothing prevents negative dark energy densities,  $f(z) < 0$ , which appear in our work as an  $\Omega_m > 1$  MLE (see also [32]), and we have witnessed an uptick in recent attempts to model the physics through negative cosmological constants, etc [56–64].

#### ACKNOWLEDGMENTS

This article/publication is based upon work from COST Action CA21136 – “Addressing observational tensions in cosmology with systematics and fundamental physics (CosmoVerse)”, supported by COST (European Cooperation in Science and Technology). SP would like to acknowledge the support of the Iran National Science Foundation (INSF) post-doctoral funds under project No. 4024802. MMSHJ acknowledges support from the ICTP through the senior Associates Programme (2023–2028) and as well as funds from ICTP HECAP section.

## Appendix A: Non-flat $\Lambda$ CDM

In this appendix we explore the implications for curvature  $\Omega_k$  of varying the effective redshift of the DES 5YR sample. The motivation for studying curvature is that it scales as  $(1+z)^2$ , versus  $(1+z)^3$  for pressureless matter and  $(1+z)^0$  for the cosmological constant, which makes it more relevant than dark energy at higher redshifts in the late Universe. Explicitly, the non-flat  $\Lambda$ CDM Hubble parameter is

$$H(z) = H_0 \sqrt{1 - \Omega_m - \Omega_k + \Omega_k(1+z)^2 + \Omega_m(1+z)^3}, \quad (\text{A1})$$

where one should now replace  $\chi(z)$  in (2) with

$$\chi_k(z) := \begin{cases} \frac{1}{\sqrt{\Omega_k}} \sinh(\sqrt{\Omega_k} \chi(z)) & \Omega_k > 0 \\ \chi(z) & \Omega_k = 0 \\ \frac{1}{\sqrt{-\Omega_k}} \sin(\sqrt{-\Omega_k} \chi(z)) & \Omega_k < 0 \end{cases} \quad (\text{A2})$$

where  $\chi(z)$  is still defined in (2).

We will see that the DES sample strongly embraces a closed Universe at higher redshifts. How this is connected to CMB anomalies pointing to  $\Omega_k < 0$  [65, 66] is an open question. Nevertheless, here the interpretation is relatively clear. As noted in [67], the Risaliti-Lusso QSOs [16, 17] prefer  $\Omega_k < 0$  at higher redshift, e. g. [25], as a means of decreasing the luminosity distance relative to the Planck flat- $\Lambda$ CDM case (due to the sine function in (A2)); a similar effect should be at work here.

In Fig. 3 we show the profile likelihood ratios, where cyan denotes the full DES 5YR sample including the 194 CfA/CSP/Foundation SNe [47–50], whereas black corresponds to the 1635 DES SNe on their own. To construct the plot we have imposed uniform priors  $H_0 \in [0, 200]$ ,  $\Omega_m \in [0, 1]$ , while scanning over  $\Omega_k$  in the range  $\Omega_k \in [-1, 1]$ . Note, our priors are wider than the DES priors  $\Omega_k \in [-0.5, 0.5]$  [39], and we have made sure when we minimise the  $\chi^2$  with respect to  $(H_0, \Omega_m)$  that the MLE are not impacted by our bounds on the auxiliary parameters  $(H_0, \Omega_m)$ . We remark also that since our prior is not physically motivated and there is no boundary between our MLEs and  $\Omega_k = 0$ , the Feldman-Cousins prescription [52] is not relevant.

The first thing to note from Table II is that when we use the full sample, we agree with Table 2 of [39] that  $\Omega_m = 0.16 \pm 0.16$ . Slight disagreements are due to the fact that we have only sampled  $\Omega_k$  at approximately 100 evenly spaced  $\Omega_k$  values and we expect that one can improve agreement by increasing the number of  $\Omega_k$  where we minimise the  $\chi^2$ . Thus, the cyan profile likelihood in Fig. 3 is in line with expectations. Nevertheless, as we remove the low redshift SNe, starting with the 194 SNe common to the CfA/CSP/Foundation samples [47–50], the profile likelihood peak or MLE shifts to negative  $\Omega_k$  values. Noting that  $\Omega_k = 0$  recovers our findings in the main text, we recognise that the fit to data can be improved through  $\Omega_k < 0$ . For the highest redshift SNe  $z > 0.8$ , the  $\chi^2$  improvement is not great, as is evident from the red curve in Fig. 3. Nevertheless, the improvement is non-negligible at lower redshifts and is extremely pronounced for DES SNe with  $z > 0.5$ , as demonstrated by the green curve in

Fig. 3. From Table II, once one excludes the lowest redshift SNe in the CfA/CSP/Foundation samples, it is evident that DES SNe on their own prefer a closed Universe with  $\Omega_k < 0$ .

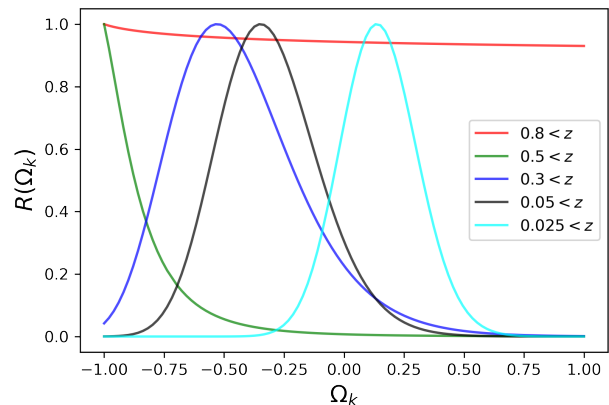


FIG. 3: Profile likelihood ratios for curvature  $\Omega_k$  with increasing effective redshift. The cyan and black profiles differ only in the addition of SNe from external data sets to the DES 5YR SNe sample.

We can drill down on this discrepancy a bit more. Invoking Wilks’ theorem [44] and following a similar analysis as in the main text, a flat Universe appears at  $\Delta\chi^2 = 0.89, 2.5, 3.1, 10.0, 0.1$ , corresponding to  $0.9\sigma, 1.6\sigma, 1.8\sigma, 3.2\sigma, 0.3\sigma$  for the cyan, black, blue, green and red profile likelihoods, respectively. For the lowest redshifts probed in Fig. 3 it is clear that profile likelihoods are close to Gaussian, so we expect this to be a good approximation. For  $z > 0.5$  our boundary at  $\Omega_k = -1$  prevents us from finding the MLE, but it is obvious that it appears at  $\Omega_k < -1$ . Nevertheless, assuming that the profile likelihood peak appears at  $\Omega_k = -1$  allows us to get a *lower bound* on any discrepancy with the flat Universe. This bounds the preference for a closed Universe from DES SNe with  $z > 0.5$  below at  $3.2\sigma$ . Note, there is nothing unphysical about  $\Omega_k < -1$  parameter space, so one could simply relax the priors, as we have done in the text, to find the MLE or profile likelihood peak, which would invariably exacerbate the tension.

Redshift	# SNe	$\Omega_k$ (68%)	$\Omega_k$ ( $\Delta\chi^2 \leq 1$ )
0.025 < z	1829	$0.13^{+0.16}_{-0.16}$	$0.13^{+0.16}_{-0.14}$
0.05 < z	1635	$-0.35^{+0.24}_{-0.18}$	$-0.35^{+0.22}_{-0.18}$
0.3 < z	1426	$-0.54^{+0.30}_{-0.22}$	$-0.54^{+0.28}_{-0.22}$
0.5 < z	874	< -0.80 (-1)	< -0.91 (-1)
0.8 < z	128	< 1 (-1)	< 1 (-1)

TABLE II: 68% confidence intervals inferred with two methods from DES SNe in different redshift ranges. The number of SNe are also documented. For one-sided confidence intervals we record the MLE in brackets.

We can get an alternative handle on the discrepancies by in-

tegrating under the (normalised) profile likelihood ratio curve as outlined in the text. Doing so, we find a flat Universe is located at  $0.9\sigma$ ,  $1.6\sigma$ ,  $1.7\sigma$ ,  $2.5\sigma$ ,  $0.7\sigma$  for the cyan, black, blue, green and red profile likelihoods, respectively. Where we find good agreement between the methods, it is expected since Wilks' theorem assumes profile likelihoods are Gaussian, an assumption that is valid in the large sample limit. Evidently, 1426, 1635 and 1829 SNe samples (see Table II) are large enough, since the profile likelihood are visibly Gaussian

in Fig. 3. Samples of 128 and 874 SNe may also be large samples and whether Wilks' theorem is a valid approximation can only be judged by relaxing the  $\Omega_k$  priors to locate the MLE or profile likelihood peak. Understandably, the greatest difference in statistical significance between the profile likelihood ratio confidence levels arises where the profile likelihood is impacted by the  $\Omega_k = -1$  bound. However, what is important here is that different methods can distinguish insignificant discrepancies ( $\lesssim 1\sigma$ ) from more significant tensions ( $\gtrsim 2.5\sigma$ ).

- 
- [1] E. Di Valentino, O. Mena, S. Pan, L. Visinelli, W. Yang, A. Melchiorri, D. F. Mota, A. G. Riess, and J. Silk, "In the realm of the Hubble tension—a review of solutions," *Class. Quant. Grav.* **38** (2021), no. 15, 153001, [2103.01183](#).
- [2] L. Perivolaropoulos and F. Skara, "Challenges for  $\Lambda$ CDM: An update," *New Astron. Rev.* **95** (2022) 101659, [2105.05208](#).
- [3] E. Abdalla *et al.*, "Cosmology intertwined: A review of the particle physics, astrophysics, and cosmology associated with the cosmological tensions and anomalies," *JHEAp* **34** (2022) 49–211, [2203.06142](#).
- [4] C. Krishnan, E. Ó Colgáin, M. M. Sheikh-Jabbari, and T. Yang, "Running Hubble Tension and a  $H_0$  Diagnostic," *Phys. Rev. D* **103** (2021), no. 10, 103509, [2011.02858](#).
- [5] C. Krishnan and R. Mondol, " $H_0$  as a Universal FLRW Diagnostic," [2201.13384](#).
- [6] K. C. Wong *et al.*, "H0LICOW – XIII. A 2.4 per cent measurement of  $H_0$  from lensed quasars:  $5.3\sigma$  tension between early- and late-Universe probes," *Mon. Not. Roy. Astron. Soc.* **498** (2020), no. 1, 1420–1439, [1907.04869](#).
- [7] M. Millon *et al.*, "TDCOSMO. I. An exploration of systematic uncertainties in the inference of  $H_0$  from time-delay cosmography," *Astron. Astrophys.* **639** (2020) A101, [1912.08027](#).
- [8] C. Krishnan, E. Ó Colgáin, Ruchika, A. A. Sen, M. M. Sheikh-Jabbari, and T. Yang, "Is there an early Universe solution to Hubble tension?," *Phys. Rev. D* **102** (2020), no. 10, 103525, [2002.06044](#).
- [9] M. G. Dainotti, B. De Simone, T. Schiavone, G. Montani, E. Rinaldi, and G. Lambiase, "On the Hubble constant tension in the SNe Ia Pantheon sample," *Astrophys. J.* **912** (2021), no. 2, 150, [2103.02117](#).
- [10] M. G. Dainotti, B. De Simone, T. Schiavone, G. Montani, E. Rinaldi, G. Lambiase, M. Bogdan, and S. Ugale, "On the Evolution of the Hubble Constant with the SNe Ia Pantheon Sample and Baryon Acoustic Oscillations: A Feasibility Study for GRB-Cosmology in 2030," *Galaxies* **10** (2022), no. 1, 24, [2201.09848](#).
- [11] J.-P. Hu and F. Y. Wang, "Revealing the late-time transition of  $H_0$ : relieve the Hubble crisis," *Mon. Not. Roy. Astron. Soc.* **517** (2022), no. 1, 576–581, [2203.13037](#).
- [12] E. Ó Colgáin, M. M. Sheikh-Jabbari, R. Solomon, G. Bargiacchi, S. Capozziello, M. G. Dainotti, and D. Stojkovic, "Revealing intrinsic flat  $\Lambda$ CDM biases with standardizable candles," *Phys. Rev. D* **106** (2022), no. 4, L041301, [2203.10558](#).
- [13] E. Ó Colgáin, M. M. Sheikh-Jabbari, R. Solomon, M. G. Dainotti, and D. Stojkovic, "Putting flat  $\Lambda$ CDM in the (Redshift) bin," *Phys. Dark Univ.* **44** (2024) 101464, [2206.11447](#).
- [14] X. D. Jia, J. P. Hu, and F. Y. Wang, "Evidence of a decreasing trend for the Hubble constant," *Astron. Astrophys.* **674** (2023) A45, [2212.00238](#).
- [15] X. D. Jia, J. P. Hu, and F. Y. Wang, "Uncorrelated estimations of  $H_0$  redshift evolution from DESI baryon acoustic oscillation observations," [2406.02019](#).
- [16] G. Risaliti and E. Lusso, "Cosmological constraints from the Hubble diagram of quasars at high redshifts," *Nature Astron.* **3** (2019), no. 3, 272–277, [1811.02590](#).
- [17] E. Lusso *et al.*, "Quasars as standard candles III. Validation of a new sample for cosmological studies," *Astron. Astrophys.* **642** (2020) A150, [2008.08586](#).
- [18] S. Pourojaghi, N. F. Zabihi, and M. Malekjani, "Can high-redshift Hubble diagrams rule out the standard model of cosmology in the context of cosmography?," *Phys. Rev. D* **106** (2022), no. 12, 123523, [2212.04118](#).
- [19] E. Pastén and V. H. Cárdenas, "Testing  $\Lambda$ CDM cosmology in a binned universe: Anomalies in the deceleration parameter," *Phys. Dark Univ.* **40** (2023) 101224, [2301.10740](#).
- [20] O. Akarsu, E. Ó Colgáin, A. A. Sen, and M. M. Sheikh-Jabbari, " $\Lambda$ CDM Tensions: Localising Missing Physics through Consistency Checks," [2402.04767](#).
- [21] G. Risaliti and E. Lusso, "A Hubble Diagram for Quasars," *Astrophys. J.* **815** (2015) 33, [1505.07118](#).
- [22] E. Ó Colgáin, M. M. Sheikh-Jabbari, and L. Yin, "Do high redshift QSOs and GRBs corroborate JWST?," *arXiv e-prints* (May, 2024) arXiv:2405.19953, [2405.19953](#).
- [23] T. Yang, A. Banerjee, and E. Ó Colgáin, "Cosmography and flat  $\Lambda$ CDM tensions at high redshift," *Phys. Rev. D* **102** (2020), no. 12, 123532, [1911.01681](#).
- [24] N. Khadka and B. Ratra, "Using quasar X-ray and UV flux measurements to constrain cosmological model parameters," *Mon. Not. Roy. Astron. Soc.* **497** (2020), no. 1, 263–278, [2004.09979](#).
- [25] N. Khadka and B. Ratra, "Determining the range of validity of quasar X-ray and UV flux measurements for constraining cosmological model parameters," *Mon. Not. Roy. Astron. Soc.* **502** (2021), no. 4, 6140–6156, [2012.09291](#).
- [26] A. G. Riess *et al.*, "A Comprehensive Measurement of the Local Value of the Hubble Constant with 1 km/s/Mpc Uncertainty from the Hubble Space Telescope and the SHOES Team," *Astrophys. J. Lett.* **934** (2022), no. 1, L7, [2112.04510](#).
- [27] N. Khadka and B. Ratra, "Do quasar X-ray and UV flux measurements provide a useful test of cosmological models?," *Mon. Not. Roy. Astron. Soc.* **510** (2022), no. 2, 2753–2772, [2107.07600](#).
- [28] N. Khadka, M. Zajaček, R. Prince, S. Panda, B. Czerny, M. L. Martínez-Aldama, V. K. Jaiswal, and B. Ratra, "Quasar UV/X-ray relation luminosity distances are shorter than reverberation-measured radius–luminosity relation luminosity distances," *Mon. Not. Roy. Astron. Soc.* **522** (2023), no. 1,

- 1247–1264, [2212.10483](#).
- [29] J. Singal, S. Mutchnick, and V. Petrosian, “The X-Ray Luminosity Function Evolution of Quasars and the Correlation between the X-Ray and Ultraviolet Luminosities,” *Astrophys. J.* **932** (2022), no. 2, 111, [2203.13374](#).
- [30] V. Petrosian, J. Singal, and S. Mutchnick, “Can the Distance-Redshift Relation be Determined from Correlations between Luminosities?,” *Astrophys. J. Lett.* **935** (2022), no. 1, L19, [2205.07981](#).
- [31] M. Zajaček, B. Czerny, N. Khadka, M. L. Martínez-Aldama, R. Prince, S. Panda, and B. Ratra, “Effect of Extinction on Quasar Luminosity Distances Determined from UV and X-Ray Flux Measurements,” *Astrophys. J.* **961** (2024), no. 2, 229, [2305.08179](#).
- [32] M. Malekjani, R. M. Conville, E. Ó Colgáin, S. Pourojaghi, and M. M. Sheikh-Jabbari, “On redshift evolution and negative dark energy density in Pantheon + Supernovae,” *Eur. Phys. J. C* **84** (2024), no. 3, 317, [2301.12725](#).
- [33] **Pan-STARRS1** Collaboration, D. M. Scolnic *et al.*, “The Complete Light-curve Sample of Spectroscopically Confirmed SNe Ia from Pan-STARRS1 and Cosmological Constraints from the Combined Pantheon Sample,” *Astrophys. J.* **859** (2018), no. 2, 101, [1710.00845](#).
- [34] D. Scolnic *et al.*, “The Pantheon+ Analysis: The Full Data Set and Light-curve Release,” *Astrophys. J.* **938** (2022), no. 2, 113, [2112.03863](#).
- [35] D. Brout *et al.*, “The Pantheon+ Analysis: Cosmological Constraints,” *Astrophys. J.* **938** (2022), no. 2, 110, [2202.04077](#).
- [36] **SNLS** Collaboration, A. Conley *et al.*, “Supernova Constraints and Systematic Uncertainties from the First 3 Years of the Supernova Legacy Survey,” *Astrophys. J. Suppl.* **192** (2011) 1, [1104.1443](#).
- [37] **SNLS** Collaboration, M. Sullivan *et al.*, “SNLS3: Constraints on Dark Energy Combining the Supernova Legacy Survey Three Year Data with Other Probes,” *Astrophys. J.* **737** (2011) 102, [1104.1444](#).
- [38] D. Brout *et al.*, “The Pantheon+ Analysis: SuperCal-fragilistic Cross Calibration, Retrained SALT2 Light-curve Model, and Calibration Systematic Uncertainty,” *Astrophys. J.* **938** (2022), no. 2, 111, [2112.03864](#).
- [39] **DES** Collaboration, T. M. C. Abbott and et al, “The dark energy survey: Cosmology results with 1500 new high-redshift type ia supernovae using the full 5-year dataset,” [2401.02929](#).
- [40] D. Rubin *et al.*, “Union Through UNITY: Cosmology with 2,000 SNe Using a Unified Bayesian Framework,” [2311.12098](#).
- [41] **DESI** Collaboration, A. G. Adame *et al.*, “DESI 2024 VI: Cosmological Constraints from the Measurements of Baryon Acoustic Oscillations,” [2404.03002](#).
- [42] **Planck** Collaboration, N. Aghanim *et al.*, “Planck 2018 results. VI. Cosmological parameters,” *Astron. Astrophys.* **641** (2020) A6, [1807.06209](#). [Erratum: *Astron. Astrophys.* 652, C4 (2021)].
- [43] R. Trotta, “Bayesian Methods in Cosmology,” [1701.01467](#).
- [44] S. S. Wilks, “The Large-Sample Distribution of the Likelihood Ratio for Testing Composite Hypotheses,” *The Annals of Mathematical Statistics* **9** (1938), no. 1, 60 – 62.
- [45] A. Gómez-Valent, “Fast test to assess the impact of marginalization in Monte Carlo analyses and its application to cosmology,” *Phys. Rev. D* **106** (2022), no. 6, 063506, [2203.16285](#).
- [46] E. Ó Colgáin, S. Pourojaghi, M. M. Sheikh-Jabbari, and D. Sherwin, “MCMC Marginalisation Bias and  $\Lambda$ CDM tensions,” [2307.16349](#).
- [47] M. Hicken, P. Challis, S. Jha, R. P. Kirsher, T. Matheson, M. Modjaz, A. Rest, and W. M. Wood-Vasey, “CfA3: 185 Type Ia Supernova Light Curves from the CfA,” *Astrophys. J.* **700** (2009) 331–357, [0901.4787](#).
- [48] M. Hicken *et al.*, “CfA4: Light Curves for 94 Type Ia Supernovae,” *Astrophys. J. Suppl.* **200** (2012) 12, [1205.4493](#).
- [49] K. Krisciunas *et al.*, “The Carnegie Supernova Project I: Third Photometry Data Release of Low-Redshift Type Ia Supernovae and Other White Dwarf Explosions,” *Astron. J.* **154** (2017), no. 5, 211, [1709.05146](#).
- [50] R. J. Foley *et al.*, “The Foundation Supernova Survey: Motivation, Design, Implementation, and First Data Release,” *Mon. Not. Roy. Astron. Soc.* **475** (2018), no. 1, 193–219, [1711.02474](#).
- [51] L. Herold, E. G. M. Ferreira, and E. Komatsu, “New Constraint on Early Dark Energy from Planck and BOSS Data Using the Profile Likelihood,” *Astrophys. J. Lett.* **929** (2022), no. 1, L16, [2112.12140](#).
- [52] G. J. Feldman and R. D. Cousins, “A Unified approach to the classical statistical analysis of small signals,” *Phys. Rev. D* **57** (1998) 3873–3889, [physics/9711021](#).
- [53] M. Moresco *et al.*, “Unveiling the Universe with emerging cosmological probes,” *Living Rev. Rel.* **25** (2022), no. 1, 6, [2201.07241](#).
- [54] **DESI** Collaboration, K. Lodha *et al.*, “DESI 2024: Constraints on Physics-Focused Aspects of Dark Energy using DESI DR1 BAO Data,” [2405.13588](#).
- [55] **DES** Collaboration, R. Camilleri *et al.*, “The dark energy survey supernova program: Investigating beyond- $\Lambda$ cdm,” [2406.05048](#).
- [56] K. Dutta, Ruchika, A. Roy, A. A. Sen, and M. M. Sheikh-Jabbari, “Beyond  $\Lambda$ CDM with low and high redshift data: implications for dark energy,” *Gen. Rel. Grav.* **52** (2020), no. 2, 15, [1808.06623](#).
- [57] L. Visinelli, S. Vagnozzi, and U. Danielsson, “Revisiting a negative cosmological constant from low-redshift data,” *Symmetry* **11** (2019), no. 8, 1035, [1907.07953](#).
- [58] R. Calderón, R. Gannouji, B. L’Huillier, and D. Polarski, “Negative cosmological constant in the dark sector?,” *Phys. Rev. D* **103** (2021), no. 2, 023526, [2008.10237](#).
- [59] G. Acquaviva, O. Akarsu, N. Katirci, and J. A. Vazquez, “Simple-graduated dark energy and spatial curvature,” *Phys. Rev. D* **104** (2021), no. 2, 023505, [2104.02623](#).
- [60] O. Akarsu, S. Kumar, E. Özulker, J. A. Vazquez, and A. Yadav, “Relaxing cosmological tensions with a sign switching cosmological constant: Improved results with Planck, BAO, and Pantheon data,” *Phys. Rev. D* **108** (2023), no. 2, 023513, [2211.05742](#).
- [61] O. Akarsu, E. Di Valentino, S. Kumar, R. C. Nunes, J. A. Vazquez, and A. Yadav, “ $\Lambda_s$ CDM model: A promising scenario for alleviation of cosmological tensions,” [2307.10899](#).
- [62] O. Akarsu, A. De Felice, E. Di Valentino, S. Kumar, R. C. Nunes, E. Ozulker, J. A. Vazquez, and A. Yadav, “ $\Lambda_s$ CDM cosmology from a type-II minimally modified gravity,” [2402.07716](#).
- [63] **DESI** Collaboration, R. Calderon *et al.*, “DESI 2024: Reconstructing Dark Energy using Crossing Statistics with DESI DR1 BAO data,” [2405.04216](#).
- [64] H. Wang, Z.-Y. Peng, and Y.-S. Piao, “Can recent desi bao measurements accommodate a negative cosmological constant?,” 2024.

- [65] W. Handley, “Curvature tension: evidence for a closed universe,” *Phys. Rev. D* **103** (2021), no. 4, L041301, [1908.09139](#).
- [66] E. Di Valentino, A. Melchiorri, and J. Silk, “Planck evidence for a closed Universe and a possible crisis for cosmology,” *Nature Astron.* **4** (2019), no. 2, 196–203, [1911.02087](#).
- [67] O. Luongo, M. Muccino, E. Ó Colgáin, M. M. Sheikh-Jabbari, and L. Yin, “Larger  $H_0$  values in the CMB dipole direction,” *Phys. Rev. D* **105** (2022), no. 10, 103510, [2108.13228](#).